Quenching Dynamics in CdSe Nanoparticles: Surface-Induced Defects upon Dilution.

Lucia Hartmann,[†] Abhishek Kumar,[‡] Matthias Welker,[§] Angela Fiore,[†] Carine Julien-Rabant,[‡] Marina Gromova,[⊥] Michel Bardet,[⊥] Peter Reiss,[†] Paul N.W. Baxter,[§] Frédéric Chandezon,[†] and Robert B. Pansu[‡,*]

[†]Laboratoire d'Electronique Moléculaire, Organique et Hybride (LEMOH), INAC/SPrAM UMR 5819 (CEA-CNRS-UJF), CEA Grenoble, 17, rue des Martyrs, F-38054 Grenoble, France, [‡]ENS Cachan, CNRS, UMR no. 8531 and IFR d'Alembert IFR 121, F-94235 Cachan, France, [§]Institut Charles Sadron, CNRS-Université de Strasbourg, F-67034 Strasbourg, France, and [⊥]Service de Chimie Inorganique et Biologique (SCIB), UMR-E CEA/UJF Grenoble, INAC CEA Grenoble, 17, rue des Martyrs, F-38054 Grenoble, France

ABSTRACT We have analyzed the decays of the fluorescence of colloidal CdSe quantum dots (QDs) suspensions during dilution and titration by the ligands. A ligand shell made of a combination of trioctylphosphine (TOP), oleylamine (OA), and stearic acid (SA) stabilizes the as-synthesized QDs. The composition of the shell was analyzed and quantified using high resolution liquid state 1H nuclear magnetic resonance (NMR) spectroscopy. A quenching of the fluorescence of the QDs is observed upon removal of the ligands by diluting the stock solution of the QDs. The fluorescence is restored by the addition of TOP. We analyze the results by assuming a binomial distribution of quenchers among the QDs and predict a linear trend in the time-resolved fluorescence decays. We have used a nonparametric analysis to show that for our QDs, 3.0 ± 0.1 quenching sites per QD on average are revealed by the removal of TOP. We moreover show that the quenching rates of the quenching sites add up. The decay per quenching site can be compared with the decay at saturation of the dilution effect. This provides a value of 2.88 ± 0.02 for the number of quenchers per QD. We extract the quenching dynamics of one site. It appears to be a process with a distribution of rates that does not involve the ligands.

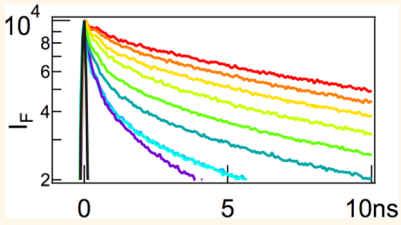

KEYWORDS: fluorescence dynamics · quantum dot · binomial distribution · ligand adsorption · Blumen_Klafter Law · CdSe

Despite constant improvements in their synthesis,[1,2] the time-resolved fluorescence decay of CdSe nanocrystals remains a complex and poorly understood process whose details are moreover strongly dependent on the synthesis procedure and on the nature of the ligand shell covering these quantum dots (QDs).[3−6] The size distribution of the nanocrystals is commonly invoked to explain the multiexponential nature of the decays. But the presence of ground state dipoles,[4] variation in surface passivation[7,8] or distribution of traps energies[9] have also been mentioned. K. E. Knowles *et al.* have shown that the fluorescence is produced by the recombination of free electrons with trapped holes[10] but the trapping of electrons is also mentioned.[11] Part of the complexity of the effect of ligand exchange on the QD fluorescence yield has been handled by a Perrin model and a Poisson distribution of quenchers.[12−14] A.J. Morris-Cohen *et al.* proposed a double binomial distribution to describe (i) the number of available sites per QD and (ii) the partial occupation of these sites by acid-derivatized viologen ligands.[15] These authors have included the binomial distribution of quenchers to analyze the electron transfer rate between QDs and viologen, assuming an exponential kinetics.[16] The use of a Poisson distribution of quenchers for the analysis of time-resolved fluorescence have been done by Tachiya.[17] But to the best of our knowledge, the binomial distribution has not been used to analyze the dynamics of the fluorescence decays of neat QD nanocrystals or using nonexponential quenching.

In this contribution, we extend the formalism by Blumen[18] and Klafter[19] to demonstrate the existence of a linear behavior in the kinetics of fluorescence using a binomial distributions of quenchers in the case of time-dependent rate coefficients. The logarithm of the decay depends linearly on the number of quenchers. We then use a nonparametric data analysis[20] that shows that beyond the complexity due to the binomial distribution of quenchers, the quenching dynamics induced by one site is multiexponential. We make profit of this analysis to study the effect of dilution on the fluorescence decay in the case of a colloidal dispersion of as-synthesized spherical

* Address correspondence to robert.pansu@ppsm.ens-cachan.fr.

Received for review July 14, 2012 and accepted September 25, 2012.

Published online September 25, 2012
10.1021/nn303150j

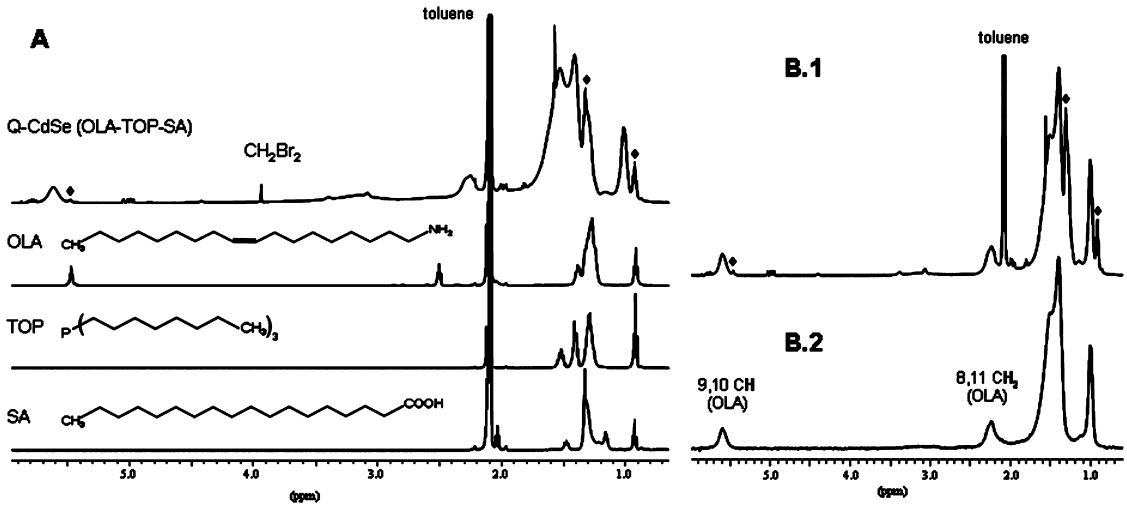

Figure 1. (A) ^{1}H NMR spectra of a CdSe QD solution ([QDs] = 62.5 μM) and of the free ligands in toluene-d_8. (B) Diffusion-filtered ^{1}H NMR spectra of CdSe QD sample. The diffusion time is Δ = 150 ms, the gradient pulse duration is δ = 2 s, and the gradient strength g = 5% (B.1) and 95% (B.2) of the maximum value achievable of 50.5 G/cm. The peaks labeled with the diamond (◊) correspond to the free ligands.

CdSe QDs (diameter = 4.81 nm) stabilized by a ligand shell composed of a mixture of trioctyl phosphine (TOP), oleylamine (OLA), and stearic acid (SA). From the analysis of the effect of dilution on the fluorescence decays traces, we show that the dilution reveals a maximum of $m = 3.0 \pm 0.1$ quencher per QD. Our approach allows us to extract the quenching dynamics of one site that shows a strong heterogeneity of the QDs.

RESULTS AND DISCUSSION

Liquid-State NMR Analysis of the Ligand Shell of the QDs. The spherical colloidal CdSe QDs were synthesized using a gram-scale protocol. The size distribution analysis conducted on TEM images (see Supporting Information) show that we have particles of $\varnothing \approx 4.81$ nm with a standard deviation of 0.29 nm (6%). This narrow size polydispersity is also confirmed by the 30 nm FWHM of the emission spectra. The as-synthesized QDs are covered by a ligand shell composed of a mixture of TOP, OLA, and SA whose relative proportions can significantly differ from those in the initial reaction mixture due to different affinities of the ligands for the surface of the QDs.[21] High-resolution liquid-state ^{1}H NMR spectroscopy is commonly used for qualitative and quantitative structural analyses of the ligand shell and to study potential dynamic exchange processes.[22−27] We applied these techniques to get more insights regarding the composition and the dynamics of the ligand shell of our QDs.

First, the ^{1}H NMR spectrum of freshly synthesized colloidal QDs is compared with the spectra of the free ligands recorded in the same solvent, namely toluene-d8 (Figure 1A). In the QDs spectrum, two sets of signals can be distinguished corresponding respectively to free ligands and to ligands bound to QDs. In the latter case, the resonances are broadened and low-field shifted relative to those measured for the free ligands. The assignment of broad signals to the QD-bound ligands was further confirmed by diffusion-filtered NMR (Figure 1B). Pulsed field gradient (PFG) ^{1}H NMR is an efficient tool for the measurement of the self-diffusion coefficient which enables the selective editing of the NMR spectra of the species according to their diffusion coefficient. As a matter of fact, when using appropriate experimental conditions, a complete disappearance of resonances corresponding to the fast diffusing species, that is, free ligands and solvent, can be observed as shown in Figure 1B.2.

TABLE 1. Concentration of Bound and Free Ligand Deduced from the NMR Analysis, Average Number per QD, and Average Density of Bound Ligands. The QD Concentration was 62.5 μM

ligand	concentration of bound ligands (mM)	concentration of free ligands (mM)	average number of ligands per QD	density of ligands (nm^{-2})
OLA	9	0.2	144	2.0
TOP	0.8	0.7	13	0.2
SA	5.8	0.6	93	1.3
total	15.6	1.5	250	3.5

To quantify the composition of the ligand shell, CH_2Br_2 was added as an internal standard. The resonance of OLA is easily distinguished from SA and TOP by the olefinic protons signal at 5.61 ppm. Using this resonance for the quantification of bound OLA, we obtain a concentration of $[OLA_{bound}] = 9 \pm 0.1$ mM. The methylene (1.3−1.8 ppm) and methyl (1.01 ppm) group resonances assigned to the bound ligands strongly overlap. Nevertheless, using the fact that the CH_2/CH_3 ratios for TOP and SA are different, and by subtracting the contribution of OLA and the free ligands to the intensity of the methylene and methyl group resonances, we estimate the concentration of bound TOP and SA to be $[TOP_{bound}] = 0.8 \pm 0.6$ mM and $[SA_{bound}] = 5.8 \pm 0.9$ mM (Table 1). The concentration

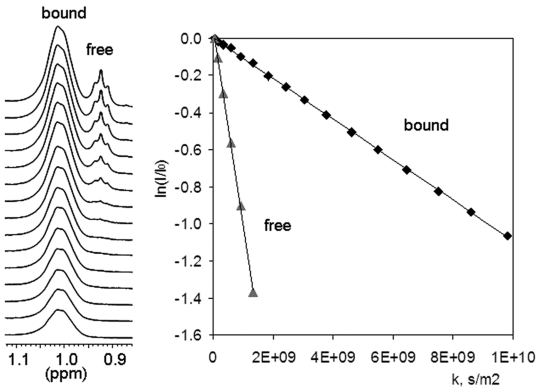

Figure 2. Attenuation profile for the CH_3 resonances (free and bound ligands) in ^1H NMR PFG spectra (Δ = 150 ms, δ = 2 ms, τ = 0.5 ms, g varying from 5% to 95% of the maximum amplitude of 50.5 G/cm); and corresponding plots of $\ln(I/I_0)$ *versus* $k = (\gamma_H g\delta)^2(\Delta - \delta/3 - \tau/2)$ for these resonances.

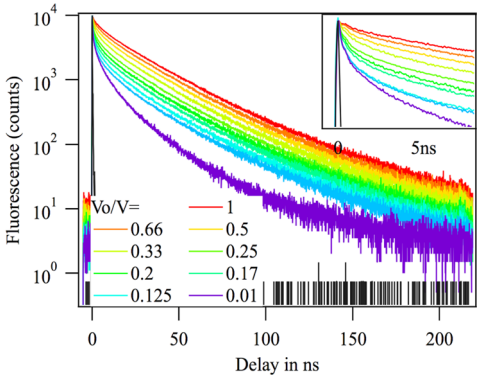

Figure 3. Fluorescence decays of a solution of QDs 41.5 μmol/L in toluene that is further diluted in toluene. Excitation wavelength: 450 nm, Detection wavelength: 634 nm with 20 nm slits. The black curve is the instrument response function. The inset shows the same curves on a smaller time scale. When diluting the stock solution, the fluorescence yield decreases as measured from the area under the decay curves. A long component remains, and the fast component develops and becomes faster. This is characteristic of a quenching by a limited number of quenchers that add their quenching rates.

of the free ligands was quantified in the same way: $[OLA_{free}]$ = 0.2 mM, $[TOP_{free}]$ = 0.7 mM, $[SA_{free}]$ = 0.6 mM. The concentration of QDs, [QDs] = 62.5 μM, was calculated from the UV–vis absorption spectrum applying the method described in ref 28. Taking into account that the surface of a spherical QD with a diameter of 4.8 nm is around 72 nm^2, we can calculate the average number of bound ligands per QD as well as the ligand density (Table 1). We find a total average density of bound ligands of 3.5 nm^{-2}. This is in good agreement with the results obtained by other groups, taking into account that in our case the ligand shell is composed of three different ligands.[22,24,26]

The second step of our NMR analysis was to perform a quantitative PFG ^1H NMR analysis. The attenuation of the NMR peaks with increasing pulsed field gradients allows us to calculate the self-diffusion coefficients of the corresponding species (D). Figure 2 shows the attenuation profile measured for CH_3 resonances of free and bound ligands. Thanks to these results and using the Stejskal-Tanner equation (see Experimental Methods), the corresponding self-diffusion coefficients of the bound ligands can be calculated with a value of $D = 1.08 \times 10^{-10}$ m s^{-2}. Using the Stokes–Einstein eq 15, we obtain a value of 7.3 nm for the hydrodynamic diameter d_H of the QDs. This corresponds well with the size of the QDs core of diameter 4.8 nm covered by the ligand shell approximately 1.2 nm thick. Therefore, PFG NMR analysis confirms the assignment of broad resonances to protons of the ligands bound to the QDs. Furthermore, the values of D calculated from the attenuation observed for the four broad peaks (Figure 1B.2) are very close (see Table S1 in Supporting Information). For the free ligands, from the plot in Figure 2 we obtain a value $D(CH_{3free}) = 1.04 \times 10^{-9}$ m s^{-2}. This is in reasonable agreement with the values of D measured for the ligands in toluene-d_8 ($D(TOP_{free}) = 0.92 \times 10^{-9}$ m s^{-2}, $D(SA_{free}) = 1.1 \times 10^{-9}$ m s^{-2}, and $D(OLA_{free}) = 1.3 \times 10^{-9}$ m s^{-2}) taking into account the different proportion of the free ligands.

Quenching by Dilution, Qualitative Approach. The QD stock solution (41.5 μmol/L calculated from the absorbance)[28] in toluene stabilized by OLA, TOP, and SA was further diluted in toluene. The decay curves are gathered in Figure 3, for an excitation wavelength at 450 nm and an emission collected from 624 to 644 nm. Upon dilution of the stock solution, a fast component appears but at the same time a long component remains. The decays at long time (<30 ns) are parallel. A fraction of the QDs still exhibits the same fluorescence lifetime of 37 ns as that of the stock solution. They are not quenched. The proportion of the populations of quenched and nonquenched QDs can be analyzed using a binomial distribution of a few quenching sites per QD (see Supporting Information).[7] Upon dilution, one may assume that ligands are removed from the surface of the QD and that surface defects are formed that act as quenchers.[10]

The inset in Figure 3 emphasizes the decay curves at short time (<10 ns). It appears that the initial decay rate increases with the dilution factor.

This behavior does not correspond to the case where the quenching rate of the QD is independent of the number of quenchers since the initial slope would remain the same when the proportion of the two populations (quenched/not quenched) is changing.[29] Here, when the number of quenchers per QD increases, we see a change in the initial slope of the decays: the quenchers add their quenching rate. This behavior of the fluorescence decays has already been observed but only the stationary fluorescence quenching was analyzed.[7] In the following we shall quantitatively explain the quenching dynamics of QDs by some quenchers.

We can see on Figure 3 that at a high dilution factor of 100, the contribution of the unquenched QD disappears. This is an indication that the number of possible

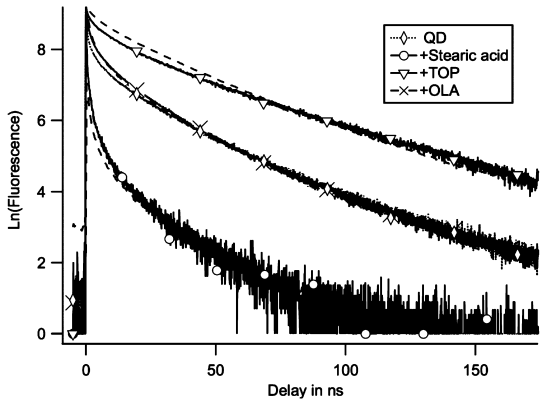

Figure 4. Fluorescence decays after addition of solvent or of ligand: (◇) solution of QDs at a concentration 20 μmol/L; (○) same with stearic acid (final concentration of added SA 0.25 mol/L); (▽) same with TOP (1.1 mol/L); (×) same with oleylamine (OLA) (1.5 mol/L). It can be seen that the presence of OLA has barely any effect on the decay curve. The fluorescence recovers upon the addition of TOP, whereas the addition of stearic acid SA induces a precipitation and an increased quenching. The measured decays are compared with the fitted decays (dashed lines) according to a Perrin model assuming that more quenching sites with the same quenching rate per site are created by the addition of SA. We can see that the addition of SA does increase the number of quenching sites but not the quenching rate per site.

quenching sites per nanoparticle is limited and that the opening of the quenching site can reach saturation.

Fluorescence Recovery. We have compared the effect of a dilution in toluene with the dilution in the three surfactants in order to indentify which ligand is responsible of the quenching. The fluorescence recovery upon the addition of ligand is summarized in Figure 4. To a volume 0.1 mL of the 41.5 μmol/L of the QD solution, we have added the same volume of toluene, or 0.1 mL of either TOP, or 0.1 mL of oleylamine OLA, or 0.1 mL of a solution of stearic acid SA at a concentration of (0.5 mol/L), and we monitored the evolution of the fluorescence decay curves in the different cases. We can see that the effect of the addition of OLA is similar to that of the addition of toluene. OLA is not involved in the quenching. The addition of TOP reduces the quenching, whereas the addition of stearic acid increases the quenching amplitude. This indicates that the quenching by dilution is due to the removal of TOP and possibly by its replacement by stearic acid.

Modeling: Binomial Distribution of Quenchers. The quenching by a small number of quenchers was first described by Perrin[30] for the static part. Tachiya addressed this question in the time-resolved case.[31,32] Infelta[33,34] Tachiya,[35] and Miller D.J.[36] have treated the quenching dynamics in the case of micelles. Tachiya has recently applied Perrin quenching for the time-resolved FRET quenching of QDs.[17] Blumen has predicted the transfer of energy of one fluorescent molecule to an ensemble of surrounding sites that are randomly occupied.[18] This has been generalized by Klafter as a first passage time problem.[37]

Here we shall use the formalism of Blumen to describe the quenching by a few quenchers eq 5−9) but we show that the average fluorescence decay per quencher in non exponential (eq 3 and that the quenching rate is proportional to the number of quenchers eq 4.

The quenching rate constant depends of the respective nature of the exciton and of the quenching site. One can assume that the hole part of the exciton is trapped after each excitation in different positions i.[38,39] A few quenching sites labeled $j \in [1,m]$ that are randomly occupied quench them. The different quenching sites j have different quenching rate k_{Qij}. The average on i and j of the quenching rate will be nonexponential eq 2 but only the average on j gives a quenching rate that increases with the number of quenchers.

The decay of one emissive site in position i is given by[18−31]

$$I_{fiK}(t) = I_{fiK}(0)\exp(-k_f t)\prod_{j=1}^{m}\exp(-\delta_{jK}k_{Qij}t) \quad (1)$$

where k_{Qij} is the quenching rate constant of a site in position i by a quencher in site j. δ_{jK} equals 1 or 0 if the quenching site j is active or not in the configuration K. k_f is the fluorescence rate constant in the absence of quencher.

The ensemble decay is the sum over all the possible K configurations of quenchers among the quenching sites but also over all the positions i of the emissive site in the QDs:

$$I_f(t) = \exp(-k_f t)\sum_i\sum_K I_{fiK}(0)\prod_{j=1}^{m}\exp(-\delta_{jK}k_{Qij}t) \quad (2)$$

The K configurations with one quencher are equiprobable. The average decay over the K configurations of 1 quencher is given by relation 3a. It can be described as a time dependent rate coefficient $k_{Qi}(t)$.[40]

$$\begin{aligned} I_{fi1}(t) &= I_{fi1}(0)/m\exp(-k_f t)\sum_{j=1}^{m}\exp(-k_{Qij}t) \\ &= I_{fi1}(0)\exp\left(-k_f t - \int_0^t k_{Qi}(u)\,du\right) \end{aligned} \quad (3)$$

In the case of our data, we shall assume that the rate coefficient is the same whatever the position i of the emissive site in the QDs: $k_Q(t)$. For n quenchers the rates add up to $n.k_Q(t)$ as shown in the Supporting Information.

$$I_{fn}(t) = I_{fn}(0)\exp\left(-k_f t - n\int_0^t k_Q(u)\,du\right) \quad (4)$$

Let us assume that the maximum number of quenching sites is m, the same for all QDs. (The case of a binomial distribution of m values is treated in ref 15 for the static quenching). The probability that a site is active for quenching is p. The number of active quenching sites per particle varies from 0 to m, leading to $m + 1$ different populations of fluorescent QDs in

proportions that follow the binomial distribution:

$$I_{fn}(0) = I_f(0) C_m^n p^n (1-p)^{m-n} \quad (5)$$

From eqs 4 and 5, the fluorescence decay of the total population will be

$$I_f(t) = \sum_{n=0}^{m} I_{fn}(t)$$
$$= I_f(0) \sum_{n=o}^{m} C_m^n p^n (1-p)^{m-n} \exp(-k_f t - n \int_o^t k_Q(u)\, du) \quad (6)$$

Thus applying the binomial theorem, we can write:

$$\frac{I_f(t)}{I_f(0)} \exp(k_f t) = \{1 + p(\exp(\int_o^t k_Q(u)\, du) - 1)\}^m \quad (7)$$

When p tends to 1, that is, when all QD have m active quenching sites:

$$\ln\left(\frac{I_f(t)}{I_f(0)}\right) + k_f t \rightarrow -m \int_o^t k_Q(u)\, du \qquad \text{as} \quad p \rightarrow 1 \quad (8)$$

When p tends to 0, the total fluorescence decay can be approximated by

$$\ln\left(\frac{I_f(t)}{I_f(0)}\right) + k_f t \simeq mp\{\exp(-\int_o^t k_Q(u)\, du) - 1\}$$
$$\text{as} \quad p \rightarrow 0 \quad (9)$$

which is the formula obtained assuming a Poisson distribution of quenchers.[41]

We have demonstrated this formula in the case of immobile reactants. We show in the Supporting Information that, in some cases, it can be applied to other types of reaction with time dependent rate coefficients such as diffusion limited reactions.

Equation 9 predicts a behavior that agrees with our qualitative analysis. The amplitude of the quenching term {between braces} is multiplied by the number of quenchers mp. The quenching term vanishes at long time leaving an unquenched decay with a decay rate k_f independent of quencher concentration.

Data Treatment and Quantitative Analysis. As long as p, the occupation probability of the quenching sites, remains low, the logarithm of the fluorescence decays should depend linearly on mp as shown by eq 9. The function $\int k_Q(u)\, du$ is unknown but can be obtained using a principal component analysis to this linear problem.[20,42] We used the data analysis environment Igor Pro from Wavemetrics.[43] The PCA helps in analyzing curves as a linear combination of reference curves. The decays are considered as vectors in a space of 4096 dimensions. The algorithm is looking for an orthonormal base on which to express the data. The first vector of the base is chosen to be the closest to the data. The data are then projected in the space orthogonal to that first vector and the successive elements of the base are constructed by recurrence. The fraction of the data described by each component is displayed in the inset of Figure 5. The inset shows that the first two components are sufficient to properly describe the data. This is confirmed by the shape of the sum of components beyond the two firsts that is shown on Figure 5. It is shapeless and contains only noise.

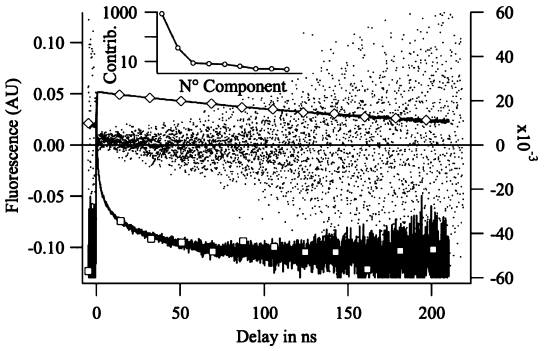

Figure 5. Theory predicts that the logarithm of the fluorescence decay in the case of the quenching by a Poisson distribution of quenchers will be the sum of two components. Indeed in the inset is displayed the contributions of the components proposed by the principal component analysis (PCA) for the description of the data. Only two have a significant contribution to the data. The sum of the contribution of the discarded components is plotted as a dotted curve. It contains more noise than kinetics. Components with a physical meaning can be built as linear combinations of the components proposed by the PCA. One combination is chosen to be as close as possible to a monoexponential decay (lozenge). It represents the fluorescence decay of QD without quencher. The second one is chosen to be flat at long times (square). This component is the decay dynamics of one site. It appears to be highly nonexponential.

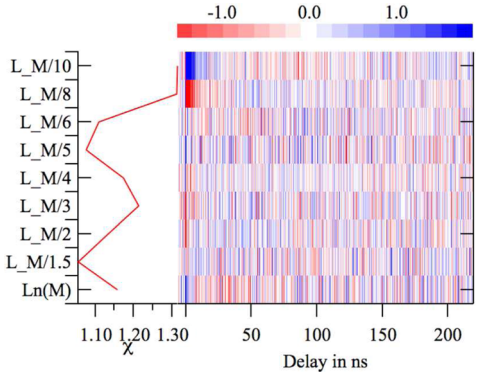

Figure 6. The quality of the description of the data by the two components is shown. First the weighted difference between the data and their description is plotted in red/white/blue color scale. It can be seen that points are randomly red or blue which means that the data are randomly above and below their description. One domain is not well described: the short time of the most diluted sample. The standard deviations of the weighted residuals are represented for each curve. It confirms that the two most diluted decays are less well described by the Poisson model.

The quality of the description of the data by the two components is depicted by the weighted residuals in Figure 6. The map made from the residuals of each curve exhibits a random change in sign. The χ^2 of the

adjustment of each curve is close to one, showing that the quality of the description of the data by the two first components is very good.

We thus show that the logarithm of the decays can be described as the sum of two curves: the quenchers add their actions and the decay rate coefficient of n quenchers is $n\int k_Q$ where $\int k_Q$ states for $\int k_Q(u)\,du$. The next step is to extract the unquenched component and the quenching component from the data. The two components that have been produced by the principal component analysis are not the two components predicted by the theory, but a linear combination of them. Any linear combination of the two main components will describe the data equally well. Thus we need to make additional hypotheses.

To describe the unquenched component, we have chosen a combination as close as possible to an exponential. We obtain a curve that describes the rise of the fluorescence during the excitation pulse and the exponential decay of the unquenched population with a lifetime of 45 ns that compares with the one measured on concentrated solutions. For the component $\int k_Q$ that describes the quenching, we have chosen a combination that tends to a horizontal slope at long time. This component represents the quenching rate per one quencher eq 9.

The adjustment of the decays on these two components $\exp(-k_f t)$ and $\int k_Q(u)\,du$ according to eq 9 give us the value for $mp = \langle n \rangle$.

Thermodynamics of the Formation of the Quenching Sites. As described in the previous section and using eq 9, we can extract the average number of quenchers per QD $< n \geq mp$ from the data analysis of the dilution experiment. Let us assume that the ligands L = (TOP or, OLA, or ST) are in equilibrium between the solution (as free ligands) and the surface of the QDs (as bound ligands):

$$rL + C_{n+1} \rightleftharpoons C_n K_{eq} \qquad (10)$$

with an equilibrium constant K_{eq} and where C_n, (C_{n+1}) stands for any one of the combinations of n, $(n + 1)$ quenching sites on a QD.

The stoichiometric coefficient r for the ligand is left unknown, since one may assume that a defect is revealed by the synergic removal of r ligands at a time. When using the chemical eq 10, we assume that the sites are identical and independent. The concentration ratio between two populations that differs by the occupation of one quenching site is equal to the ratio of the probabilities of having an empty quenching site or an occupied one:

$$\frac{[C_n]}{[C_{n+1}]} = \frac{1-p}{p} = \frac{m-\langle n \rangle}{\langle n \rangle} = K_{eq}[L]^r \qquad (11)$$

where p is the probability that a site is active for quenching. $\langle n \rangle$ is the average number of quenching sites among the m possible ones. This relation can be rewritten as

$$\frac{1}{\langle n \rangle} = \frac{1}{m} + \frac{K_{em}}{m}[L]^r \qquad (12)$$

This is the Langmuir isotherm in the case of particle dispersions.[44]

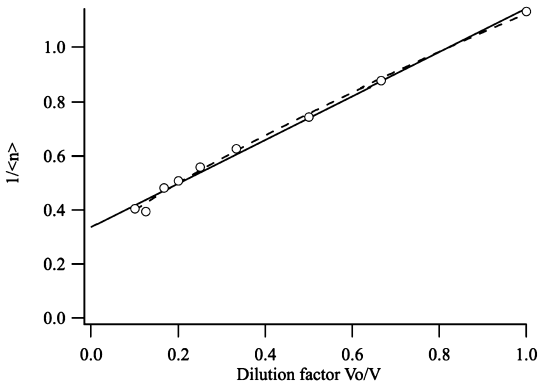

Figure 7. The average number of quenching sites obtained from the amplitude of the quenching in decays is represented *versus* the inverse of the dilution factor according to a Langmuir model. The dotted curve is an adjustment with a free stoichiometric parameter r found equal to 0.8 ± 0.1. The straight line is an adjustment with stoichiometric parameter $r = 1$. The point alignment shows that the creation of one quenching site is due to the removal of one ligand and that the maximum number of quenching sites is 2.97 ± 0.1.

In Figure 7, we obtained a straight line by plotting the inverse of the amplitude of the quenching term, $1/\langle n \rangle$, *versus* the inverse of the dilution factor V_o/V. The free ligand concentration decreases with the dilution. First, we can see that the experimental data points align on a straight line when plotted *versus* (V_o/V). This indicates that $r = 1$. Thus a quenching defect is due to the removal of one single ligand. Second, the concentration of free ligands follows linearly the dilution. This means that the large majority of ligands are tightly bound to the surface of the QD and do not feed the solution in free ligands during the dilution. Third the intercept of the fitted straight line with the Y-axis gives a value of $m = 2.97 \pm 0.1$. Thus up to three quenching sites per QD can be rendered active under our experimental conditions. This is 3 out of 13 TOP per QD on average as was measured by NMR.[45] This is much less than the 37 quenching sites measured in the case of CdSe in chloroform.[6] This could be only a fraction of the total ligand released, if the other ligands are released from sites that do not induce a quenching.

The concentrations of the free ligands have been measured by NMR. They are gathered in Table 1. From the slope of the fit in Figure 7, we can deduce an average affinity constant of all three ligands of 1600 L/mol. This is in good agreement with the results obtained by other groups, taking into account that in our case the ligand shell is composed of three different ligands.[16]

Kinetics of the Quenching. From the data treatment part, we get the shape of the time-dependent rate $\int k_Q$ of the quenching by one site. When all the QDs present

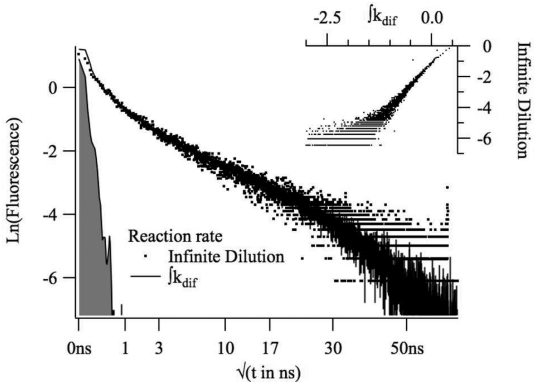

Figure 8. The quenching rate per quencher $\int k_Q$ obtained from the Poisson distribution analysis can be compared with the quenching rate at high dilution where all quenching sites are active on all QDs. In the inset, the parametric plot of the rates shows that the quenching rate at high dilution is 2.88 ± 0.02 faster than the rate per quenching sites. This perfectly agrees with the number of quenching site deduced from the Langmuir analysis. In the figure, the normalized quenching rates have been displayed as a function of √(t) together with the instrument response function (in gray).

the same maximum number of quenching sites, the decay rate of the solution will be $m\int k_Q$. This is shown by eq 8. Indeed the logarithm of the decay recorded for a solution diluted 100 times in toluene is compared to the decay rate obtained from the analysis of the first steps of the dilution in Figure 8. The scaling factor can be obtained from the plot shown in the inset where the two time functions are plotted one *versus* the other for all values of the time. We measure for the maximum number of quenching sites a value of $m = 2.88 \pm 0.02$. This confirms the value obtained by the previous thermodynamic analysis. This also validates the assumption made in the data treatment part that $\int k_Q$ is zero at long time.

The two rates are compared after scaling in Figure 8. We plot them *versus* √(time). The figure shows that ln($I(t)$) scales as $\sqrt{t}$ at short times:

$$\ln(I(t)) = a - (t/\tau_Q)^{1/2} + O((t/\tau_Q)^{3/2}) \qquad (13)$$

with a value of 160 ns for τ_Q.

We can discard some hypothesis about what is the process that is responsible for the fluorescence decay. We have compared the decay obtained in 1.1 mol/L of SA with the decay expected from an increase of the number of quenching sites with the same quenching rate per site (Figure 4). We see that the observed decay is not faster than the predicted one. The addition of SA has increased the number of quenching sites but the rate per site remains the same. The reaction responsible of the quenching cannot be the diffusion of stearic acid molecules from the solution toward a TOP free site, since the rate per site after the addition of stearic acid is not faster.

It should also not be a diffusion of a TOP molecule out of a quenching site induced by the excitation of the nanoparticles since this diffusion would scale as $1/t^{dim}$ if it diffuses freely into the surfactant layer or toluene.[19] The reaction responsible for the formation of the quenching site thus is not the reaction responsible for the quenching kinetics. The removal of a TOP acts as a tap that opens a deactivation pathway but ligands do not participate to the quenching step.

It cannot be a fast charge trapping, a process by which the electron or hole is transferred from its initial delocalized excitonic state to a state localized on a surface atom occurring at short time followed by a slow (ns) tunneling. Indeed the deactivation of the trapped exciton would not be faster if more than one surface traps are made available, whereas we show that each quenching site adds a new decay channel for the exciton. The Perrin dependence on the number of quencher shows that the surface states add their reactivity. Thus the surface defect is one of the reactants of the reaction responsible for the nonradiative decay (recombination).

The $\sqrt{t}$ dependence shows that we have a distribution of quenching rates. This reveals a heterogeneous environment: the rate of reaction of the exciton with the surface defects varies either from QD to QD or inside a QD. The mechanism by which this reaction occurs, or the origins of the heterogeneity, are beyond the scope of this contribution. Indeed the $\sqrt{t}$ kinetics that we measure could be that of a Brownian diffusion of a mobile quencher,[46] or an energy transfer through a dipolar coupling.[19]

CONCLUSION

We have been able to decrypt the complexity of the fluorescence decays of CdSe QDs during a dilution experiment thanks to the proportionality between the rate coefficient and the average number of quenchers. We have successfully used a principal component analysis that shows that up to three quenching sites appear upon dilution of our QDs dispersion. The quenching sites are created by the release of TOP molecules one by one. The number of quenching sites is obtained independently from a Langmuir isotherm and from the kinetics study of the decay curves. In addition to a binomial distribution of the quenchers, we show that the quenching dynamics scales as $\sqrt{t}$. The nature of the surface defects and the mechanism of the reaction of the quenching sites with the exciton remain unknown.

EXPERIMENTAL METHODS

Synthesis and Characterization of the CdSe QDs. Spherical CdSe QDs (diameter ≈ 4.8 nm) were synthesized using a 2-L reactor according to the procedure described in refs [1] and [45]. In brief, 8 mmol of cadmium stearate $CdSt_2$, 184 mmol of SA, 0.85 mol (280 mL) of oleylamine (OA), and 186 mL of 1-octadecene (ODE) are introduced in the 2-L reactor which is thereafter degassed

for 45 min filled with argon and heated to 250 °C. Then 100 mL of a 0.4 M TOP-Se solution are injected within 1 s using a peristaltic pump with a strong vortex mixing. The mixture is maintained at 250 °C for 15 min and then the heating source (molten salt or graphite flakes bath) is removed. The obtained CdSe QDs are purified by first adding acetone (500 mL) then methanol (200 mL) and again 300 mL of acetone. The reactor is maintained overnight at 70 °C. This allows keeping the stearic acid in its liquid phase (melting temperature around 70 °C) while the QDs precipitate at the bottom of the reactor. At the end of this step, the supernatant is removed and the precipitated QDs are recovered and redispersed in hexane. Two further steps of purification by the addition of methanol then centrifugation and redispersion are performed before using the QDs. For all the experiments presented in this work, we used colloidal dispersions of QDs in toluene (or toluene-d_8 for the NMR analysis, see below) as the solvent. The QDs are covered by a ligand shell composed of a mixture of trioctylphosphine (TOP), oleylamine(OA), and stearate (SA) whose average composition was analyzed using solution nuclear magnetic resonance spectroscopy (NMR) techniques (*vide supra*).

The absorption spectrum of the QDs shows an excitonic peak with its maximum at 602 nm which corresponds to a diameter of 4.8 nm using the relation provided in ref 28, see Supporting Information, Figure S1. This is in excellent agreement with the average QD size, as derived from transmission electron microscopy (TEM, data not shown). The size polydispersity as derived from TEM is around 13.3%. The fluorescence spectrum of the QDs peaks at $\lambda = 620$ nm with a full width at half maximum (FWHM) of 36 nm. Powder X-ray diffraction of the QDs (data not shown) confirms the hexagonal wurtzite structure of the QDs.

High Resolution Liquid State NMR Characterization of the Composition of the Ligand Shell Covering the QDs. The composition of the ligand shell was analyzed and quantified using ^{1}H nuclear magnetic resonance spectroscopy (NMR). All NMR measurements were performed with a Bruker Avance 500 spectrometer equipped with a 5 mm BBI-*xyz*-gradient probe. The spectra were recorded in toluene-d_8 at 298 K. Typical concentrations of the QD dispersions used for the NMR analysis are about 10−100 μM as determined from the UV−vis absorption spectra.[28] For the quantification of the composition of the ligand shell, CH_2Br_2 was used as an internal concentration standard. We systematically used a digital integration of the resonance lines of ^{1}H NMR relaxed spectra (recycling time of 45 s) after baseline correction with the WIN-NMR software (Bruker Biospin, Wissembourg, France). On the basis of this quantification and on the concentration of CdSe QDs from the UV−vis spectra, we can estimate the average number of ligands per QD as well the ligand density.

In pulsed field gradient (PFG) ^{1}H NMR mode, one can measure the diffusion coefficient D of a species by monitoring the attenuation of related NMR peaks when applying variable magnetic field gradients.[25,27] The diffusion filtered spectra were recorded with the standard bipolar LED pulse sequence, $\delta = 2$ ms and $\Delta = 150$ ms. The amplitude of the trapezoidal gradient pulses was varied from 5 to 90% of the maximum amplitude of 50.5 G·cm^{-1}. The attenuation of the peaks follows the Stejskal−Tanner equation:

$$\frac{I}{I_0} = \exp(-(\gamma_H g\delta)^2 D(\Delta - \delta/3 - \tau/2)) \quad (14)$$

where D is the self-diffusion coefficient of the species considered, γ_H is the proton gyromagnetic ratio, g and δ are the gradient pulse strength and duration, respectively, Δ is the diffusion delay, and finally τ is the time interval between the bipolar gradient pulses. To calculate the hydrodynamic diameter d_H from the diffusion coefficient D, we used the Stokes−Einstein formula:

$$d_H = \frac{k_B T}{3\pi\eta D} \quad (15)$$

where k_B is the Boltzmann constant and $\eta = 0.55 \times 10^{-3}$ kg s^{-1} m^{-1} is the value of the dynamic viscosity of toluene at 298 K.

Instrument. The single photon counting set up has been describe elsewhere.[47] It uses a Tsunami titanium-doped sapphire laser from Spectra Physics and a multichannel plate photomultiplier (R3809U Hamamatsu Massy, France).

Characterization. UV−vis absorption spectra were acquired on a Carry 5000 spectrophotometer. The photoluminescence spectra were obtained using a Fluorolog III spectrometer. Transmission electron microscopy imaging of the NCs was performed using a Jeol 4000 EX microscope at 400 keV operated in bright field mode.

Conflict of Interest: The authors declare no competing financial interest.

Supporting Information Available: The UV−vis absorption and photoluminescence spectra of the CdSe QDs; a binomial analysis of the nonquenched population; a discussion about the difference between mobile quenchers and mobile fluorescent sites in the case of Perrin quenching. This material is available free of charge *via* the Internet at http://pubs.acs.org.

Acknowledgment. This work was supported by the French National Research Agency ANR through the MYOSOTIS project (Grant No. ANR-08-NANO-012-01). The authors acknowledge the help of Pierre-Alain Bayle for the nuclear magnetic resonance experiments and of Michèle Soubrenie for helpful discussions.

REFERENCES AND NOTES

1. Protiere, M.; Nerambourg, N.; Renard, O.; Reiss, P. Rational Design of the Gram-Scale Synthesis of Nearly Monodisperse Semiconductor Nanocrystals. *Nanoscale Res. Lett.* **2011**, *6*, 472–485.
2. Rogach, A. L., Semiconductor Nanocrystal Quantum Dots: Synthesis, Assembly, *Spectroscopy and Applications*; Springer Verlag: Wien, Germany, 2008.
3. Mei, B. C.; Wang, J.; Qiu, Q.; Heckler, T.; Petrou, A.; Mountziaris, T. J. Dilution Effects on the Photoluminescence of ZnSe Quantum-Dot Dispersions. *Appl. Phys. Lett.* **2008**, *93*, 083114–083116.
4. Al Salman, A.; Tortschanoff, A.; van der Zwan, G.; van Mourik, F.; Chergui, M. A Model for the Multi-exponential Excited-State Decay of CdSe Nanocrystals. *Chem. Phys.* **2009**, *357*, 96–101.
5. Talapin, D. V.; Rogach, A. L.; Kornowski, A.; Haase, M.; Weller, H. Highly Luminescent Monodisperse CdSe and CdSe/ZnS Nanocrystals Synthesized in a Hexadecyl-Amine−Trioctylphosphine Oxide−Trioctylphosphine Mixture. *Nano Lett.* **2001**, *1*, 207–211.
6. Knowles, K. E.; Frederick, M. T.; Tice, D. B.; Morris-Cohen, A. J.; Weiss, E. A. Colloidal Quantum Dots: Think Outside the (Particle-in-a-)Box. *J. Phys. Chem. Lett.* **2011**, *3*, 18–26.
7. Koposov, A. Y.; Szymanski, P.; Cardolaccia, T.; Meyer, T. J.; Klimov, V. I.; Sykora, M. Electronic Properties and Structure of Assemblies of CdSe Nanocrystal Quantum Dots and Ru-Polypyridine Complexes Probed by Steady State and Time-Resolved Photoluminescence. *Adv. Funct. Mater.* **2011**, *21*, 3159–3168.
8. Loumaigne, M.; Richard, A.; Laverdant, J.; Nutarelli, D.; Débarre, A. Ligand-Induced Anisotropy of the Two-Photon Luminescence of Spherical Gold Particles in Solution Unraveled at the Single Particle Level. *Nano Lett.* **2010**, *10*, 2817–2824.
9. Jones, M.; Lo, S. S.; Scholes, G. D. Signatures of Exciton Dynamics and Carrier Trapping in the Time-Resolved Photoluminescence of Colloidal CdSe Nanocrystals. *J. Phys. Chem. C* **2009**, *113*, 18632–18642.
10. Knowles, K. E.; McArthur, E. A.; Weiss, E. A. A Multi-timescale Map of Radiative and Nonradiative Decay Pathways for Excitons in CdSe Quantum Dots. *ACS Nano* **2011**, *5*, 2026–2035.
11. Kern, S. J.; Sahu, K.; Berg, M. A. Heterogeneity of the Electron-Trapping Kinetics in CdSe Nanoparticles. *Nano Lett.* **2011**, *11*, 3493–3498.
12. Koole, R.; Schapotschnikow, P.; de Mello Donegà, C.; Vlugt, T. J. H.; Meijerink, A. Time-Dependent Photoluminescence

Spectroscopy as a Tool to Measure the Ligand Exchange Kinetics on a Quantum Dot Surface. *ACS Nano* **2008**, *2*, 1703–1714.
13. Priyam, A.; Bhattacharya, S. C.; Saha, A. Volatile Interface of Biological Oxidant and Luminescent CdTe Quantum Dots: Implications in Nanodiagnostics. *Phys. Chem. Chem. Phys.* **2009**, *11*, 520–527.
14. Bullen, C.; Mulvaney, P. The Effects of Chemisorption on the Luminescence of CdSe Quantum Dots. *Langmuir* **2006**, *22*, 3007–3013.
15. Morris-Cohen, A. J.; Vasilenko, V.; Amin, V. A.; Reuter, M. G.; Weiss, E. A. Model for Adsorption of Ligands to Colloidal Quantum Dots with Concentration-Dependent Surface Structure. *ACS Nano* **2012**, *6*, 557–565.
16. Morris-Cohen, A. J.; Frederick, M. T.; Cass, L. C.; Weiss, E. A. Simultaneous Determination of the Adsorption Constant and the Photoinduced Electron Transfer Rate for a CdS Quantum Dot-Viologen Complex. *J. Am. Chem. Soc.* **2011**, *133*, 10146–10154.
17. Sadhu, S.; Tachiya, M.; Patra, A. A Stochastic Model for Energy Transfer from CdS Quantum Dots/Rods (Donors) to Nile Red Dye (Acceptors). *J. Phys. Chem. C* **2009**, *113*, 19488–19492.
18. Blumen, A. Excitation Transfer from a Donor to Acceptors in Condensed Media: A Unified Approach. *Il Nuovo Cimento Soc. Ital. Fis., B (1971−1996)* **1981**, *63*, 50–58.
19. Klafter, J.; Blumen, A. Fractal Behavior in Trapping and Reaction. *J. Chem. Phys.* **1984**, *80*, 875–877.
20. Ruckebusch, C.; Sliwa, M.; Pernot, P.; de Juan, A.; Tauler, R. Comprehensive Data Analysis of Femtosecond Transient Absorption Spectra: A Review. *J. Photochem. Photobiol., C* **2012**, *13*, 1–27.
21. Green, M. The Nature of Quantum Dots Capping Ligands. *J. Mater. Chem.* **2010**, *20*, 5797–5809.
22. Gomes, R.; Hassinen, A.; Szczygiel, A.; Zhao, Q. A.; Vantomme, A.; Martins, J. C.; Hens, Z. Binding of Phosphonic Acids to CdSe Quantum Dots: A Solution NMR Study. *J. Phys. Chem. Lett.* **2011**, *2*, 145–152.
23. Hassinen, A.; Moreels, I.; Donega, C. D.; Martins, J. C.; Hens, Z. Nuclear Magnetic Resonance Spectroscopy Demonstrating Dynamic Stabilization of CdSe Quantum Dots by Alkylamines. *J. Phys. Chem. Lett.* **2010**, *1*, 2577–2581.
24. Fritzinger, B.; Capek, R. K.; Lambert, K.; Martins, J. C.; Hens, Z. Utilizing Self-Exchange to Address the Binding of Carboxylic Acid Ligands to CdSe Quantum Dots. *J. Am. Chem. Soc.* **2010**, *132*, 10195–10201.
25. Moreels, I.; Fritzinger, B.; Martins, J. C.; Hens, Z. Surface Chemistry of Colloidal PbSe Nanocrystals. *J. Am. Chem. Soc.* **2008**, *130*, 15081–15086.
26. Ji, X. H.; Copenhaver, D.; Sichmeller, C.; Peng, X. G. Ligand Bonding and Dynamics on Colloidal Nanocrystals at Room Temperature: The Case of Alkylamines on CdSe Nanocrystals. *J. Am. Chem. Soc.* **2008**, *130*, 5726–5735.
27. Hens, Z.; Moreels, I.; Martins, J. C. *In Situ* ^{1}H NMR Study on the Trioctylphosphine Oxide Capping of Colloidal InP Nanocrystals. *ChemPhysChem* **2005**, *6*, 2578–2584.
28. Jasieniak, J.; Smith, L.; Embden, J. V.; Mulvaney, P.; Califano, M. Re-Examination of the Size-Dependent Absorption Properties of CdSe Quantum Dots. *J. Phys. Chem. C* **2009**, *113*, 19468–19474.
29. Schoutteten, L.; Denjean, P.; Pansu, R. B. Photophysics of "Calcium Green 1" *in Vitro* and in Live Cells. *Phys. Chem. Chem. Phys.* **1999**, *1*, 2463–2469.
30. Perrin, F. Loi de Décroissance du Pouvoir Fluorescent en Fonction de la Concentration. *C. R. Acad. Sci.* **1924**, *178*, 1978–1980.
31. Tachiya, M.; Mozumder, A. Decay of Trapped Electrons by Tunnelling to Scavenger Molecules in Low-Temperature Glasses. *Chem. Phys. Lett.* **1974**, *28*, 87–89.
32. Murata, S.; Tachiya, M. Refined Perrin Equation for the Analysis of Fluorescence Quenching by Electron Transfer. *Chem. Phys. Lett.* **1992**, *194*, 347–350.
33. Infelta, P. P.; Gratzel, M.; Thomas, J. K. Luminescence Decay of Hydrophobic Molecules Solubilized in Aqueous Micellar Systems—A Kinetic Model. *J. Phys. Chem.* **1974**, *78*, 190–195.
34. Tachiya, M. On the Kinetics of Luminescence Quenching in Micellar Systems. *J. Chem. Phys.* **1983**, *78*, 5282–5283.
35. Tachiya, M. Application of a Generating Function to Reaction Kinetics in Micelles. Kinetics of Quenching of Luminescent Probes in Micelles. *Chem. Phys. Lett.* **1975**, *33*, 289–292.
36. Miller, D. J.; Klein, U. K. A.; Hauser, M. Occupation Numbers in Micellar Solubilisation—An Excimer Study. *Ber. Bunsen-Ges. Phys. Chem* **1980**, *84*, 1135–1140.
37. Bénichou, O.; Chevalier, C.; Klafter, J.; Meyer, B.; Voituriez, R. Geometry-Controlled Kinetics. *Nat. Chem.* **2010**, *2*, 472–477.
38. Guyot-Sionnest, G.-S.; Philippe; Shim, M.; Matranga, C.; Hines, M. Intraband Relaxation in CdSe Quantum Dots. *Phys. Rev. B* **1999**, *60*, R2181–R2184.
39. Klimov, V. I.; McBranch, D. W.; Leatherdale, C. A.; Bawendi, M. G. Electron and Hole Relaxation Pathways in Semiconductor Quantum Dots. *Phys. Rev. B* **1999**, *60*, 13740–13749.
40. Berberan-Santos, M. N.; Bodunov, E. N.; Valeur, B. Mathematical Functions for the Analysis of Luminescence Decays with Underlying Distributions 1. Kohlrausch Decay Function (Stretched Exponential). *Chem. Phys.* **2005**, *315*, 171–182.
41. Bales, B. L.; Almgren, M. Fluorescence Quenching of Pyrene by Copper(II) in Sodium Dodecyl-Sulfate Micelles—Effect of Micelle Size as Controlled by Surfactant Concentration. *J. Phys. Chem.* **1995**, *99*, 15153–15162.
42. Abdi, H.; Williams, L. J. Principal Component Analysis. *WIREs Comput. Stat.* **2010**, *2*, 433–459.
43. WaveMetrics. http://www.wavemetrics.com/ (accessed 2011).
44. Atkins, P. W. *Physical Chemistry*, 4 ed.; Oxford University Press: Oxford, 1992; Vol. 1, p 995.
45. Hartmann, L. Elaboration et Etude de Matériaux Hybrides Orientés et Nanostructurés d'Intérêt pour l'Electronique Organique. Doctor Thesis, University de Strasbourg, **2012**.
46. Torney, D. C.; McConnell, H. M. Diffusion-Limited Reaction-Rate Theory for Two-Dimensional Systems. *Proc. R. Soc. London, A* **1983**, *387*, 147–170.
47. Schoutteten, L.; Denjean, P.; Joliff-Botrel, G.; Bernard, C.; Pansu, D.; Pansu, R. B. Developement of Measurement of Intracellular Calcium by Time-Resolved Photon Counting Fluorescence. *Photochem. Photobiol.* **1999**, *70*, 701–709.